IEEE Access
Multidisciplinary | Rapid Review | Open Access Journal

Received March 29, 2019, accepted April 24, 2019, date of publication May 7, 2019, date of current version May 21, 2019.

Digital Object Identifier 10.1109/ACCESS.2019.2915244

Design and Full-Scale Experimental Results of a Semi-Active Heave Compensation System for a 200 T Winch

WANGQIANG NIU[1], WEI GU[1], YUNFU YAN[2], AND XIANGYANG CHENG[2]

[1]Key Laboratory of Transport Industry of Marine Technology and Control Engineering, Shanghai Maritime University, Shanghai 201306, China
[2]Shanghai Zhenhua Heavy Industry Co., Ltd, Shanghai 200125, China

Corresponding author: Wangqiang Niu (wqniu@shmtu.edu.cn)

This work was supported in part by the Marine Engineering Equipment R&D and Industrialization Program of National Development and Reform Commission of China under Grant [2013] 1144, and in part by the High Technology of Ship Research Program of the Ministry of Industry and Information Technology of China under Grant [2016] 26.

ABSTRACT Lifting and lowering a load on the ocean can be a dangerous task but can be made easy and safe by adopting heave compensation (HC) devices. The design and full-scale experimental results of a 3000-m semi-active heave compensation (AHC) system for a 200-T winch are presented in this paper. First, the design requirements are given and the semi-AHC mechanism is chosen. An integrated cylinder with one passive chamber and two active chambers is designed. Then, the capacities of the passive and active chambers are determined. The hydraulic and electrical systems and the control strategies are introduced subsequently. Finally, full-scale factory tests at different sinusoidal wave periods and amplitudes show that the semi-AHC system has a displacement compensation efficiency of 92.9% met the design requirements. In-depth power analysis further shows that the active and passive chambers contribute 20.5% and 72.4% displacement compensation efficiencies, respectively. The efficiency of the passive chamber consists with the 68%–80% passive compensation efficiency from Oceanworks Company and Rexroth Company.

INDEX TERMS Integrated cylinder, passive heave, power analysis, semi-active heave compensation.

I. INTRODUCTION

Lifting and lowering a load on the ocean can be a dangerous task, especially in high seas [1], [2]. Heave compensation devices can be applied to make the task easy and safe and enlarge the window of operation. A recent thorough review on this area can be found in [3].

Heave compensation can be divided into three groups: passive heave compensation (PHC), active heave compensation (AHC), and semi-active heave compensation [3].

PHCs can be gas-backed accumulators that work as hydraulic springs to attenuate the heave motion [3]. They are simple open loop systems that do not require energy input to function. A 19.5 T standalone flying sheave PHC system developed by Oceanworks Corporation from Canada for remotely operated vehicles (ROVs) launch and recovery is reported in [4]. A simulation-based design is introduced. The factory testing shows the PHC system has an efficiency of 68 %.

AHCs can be used to further improve the efficiency [3], [5]. A motion reference unit (MRU) measures actual vessel motions. The AHC controller then calculates the motion of the actuator to counteract the heave motions. The efficiency of AHCs can be above 90 % [6], [7]. AHCs are close loop systems that require large amounts of energy. The actuator can be a hydraulic cylinder, a hydraulic motor, or an electrical motor [3], [6]. In [8], an AHC system for an offshore crane and a FFT-based heave prediction method are introduced. In [9] methods for heave prediction and trajectory plan for an AHC system are presented. Both works present experimental results by full-scale test benches from Liebherr Company of Austria; however, no information is given on the design process of AHC systems.

Semi-active heave compensation is an alternative hybrid system comprises PHCs and AHCs for reducing the power requirement of AHCs [3], [7]. In [10], a 3 T semi-active heave compensation system and a sliding mode control method are

The associate editor coordinating the review of this manuscript and approving it for publication was Haiyong Zheng.

TABLE 1. Design Parameters of the semi-active heave compensation system.

Parameters	Value	Unit
Winch load	200	T
Water depth	3000	m
Wave amplitude	±2.5	m
Wave period	8	s
Residual motion	10	%

introduced to deal with the disturbance. In [11], a scale model of a semi-active heave compensation system for deep-sea tether ROVs is presented. However, the design process of a semi-active heave compensation system is not discussed in these works.

In this study, the design philosophy of a semi-active heave compensation system for a 200 T winch is presented. An integrated cylinder with one passive chamber and two active chambers is designed. The capacities of the passive and active chambers are determined. Full-scale factory tests at different wave periods and amplitudes are performed to evaluate the compensation performance of the semi-active heave compensation system. In-depth power analysis is used to determine the contributions of the active and passive chambers.

II. DESIGN OF THE SEMI-ACTIVE HEAVE COMPENSATION SYSTEM

A. DESIGN REQUIREMENTS

Table 1 lists the key design requirements. The rated winch load, wave period, and peak-to-peak wave amplitude are 200 T, 8 s, and 5 m, respectively. The residual heave motion should be smaller than 10 %.

B. HEAVE COMPENSATION STRUCTURE

Oceanworks Corporation reports a 19.5 T standalone PHC system with a 68 % efficiency under factory testing [4]. Rexroth Corporation reports that their well-designed PHC devices can achieve efficiencies above 80 % [6]. This design has an efficiency of 90 % and thus PHC systems alone could not meet the requirements so AHC systems should be included.

A strictly active system has a potentially higher power requirement than a semi-active system [3]. In addition, a semi-active system has excellent fault-tolerant ability. Heave compensation ability is totally lost if a strictly active system has a fatal fault, whereas a semi-active system still has a compensation ability of roughly 70 % from its PHC part if its AHC part has a fatal fault. Thus, this study chooses a semi-active structure design.

C. CYLINDER STRUCTURE

A semi-active system has a PHC part (PHC cylinders) and an AHC part (AHC cylinders) [3].

A structure of one passive cylinder and one active cylinder is presented in [11], and these cylinders are connected by rods. Another structure of one passive cylinder and one active cylinder is presented in [12], and these cylinders are interfaced by an accumulator.

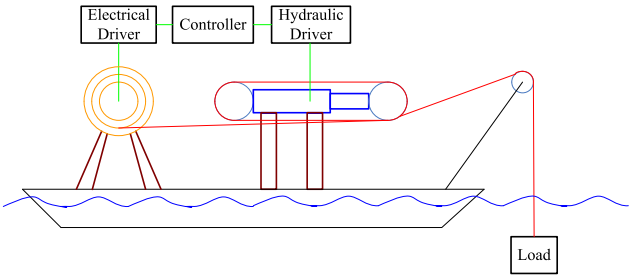

FIGURE 1. Flying sheave structure of the semi-active heave compensation system.

A structure of two large passive cylinders and one slim active cylinder is suggested in [3]. By contrast, a structure of one large passive cylinder and two slim active cylinders is reported in [10].

All the above-mentioned structures have separate cylinders for passive and active parts. In this study, a single cylinder with passive and active chambers is designed, as shown in Fig. 4. This integrated cylinder structure has a compact space and a simple sheave setting.

D. CAPACITY OF PHC AND AHC

The drag force on the cable F_{cable} in Fig. 1 is [4], [9], [10]

$$F_{cable} = W_L - B_L + W_{cable} - B_{cable} + b_L v_L |v_L| + m_L \dot{v}_L, \quad (1)$$

where W_L is the weight of a 200 T load, B_L is the buoyancy of the 200 T load, W_{cable} is the weight of the cable, B_{cable} is the buoyancy of the cable, b_L is the effective quadratic drag coefficient of the load, v_L is the load speed induced by the wave and m_L is the effective mass (real and added).

In accordance with [4], the quadratic drag force is far less than W_L, that is, $b_L v_L |v_L| \ll W_L$. From Table 1, the maximum wave induced load acceleration $\dot{v}_L$ is calculated as 1.55m/s^2, which is far less than the gravity acceleration. By neglecting the last two terms in (1), it is simplified to

$$F_{cable} \approx W_L - B_L + W_{cable} - B_{cable}. \quad (2)$$

For a typical water depth of 1500 m, the buoyancy of the 200 T load is largely cancelled by the weight and the buoyancy of the cable. After the last three terms in (2) are largely cancelled, it is changed to

$$F_{cable} \approx W_L. \quad (3)$$

The load power of the semi-active heave compensation system is

$$P_L = W_L * v_L. \quad (4)$$

From Table 1, the maximum wave induced load speed v_{Lmax} is calculated as 1.96m/s.

The peak load power of the heave compensation system is

$$P_{L\max} = W_L * v_{L\max} = 3.84 \text{ MW}. \quad (5)$$

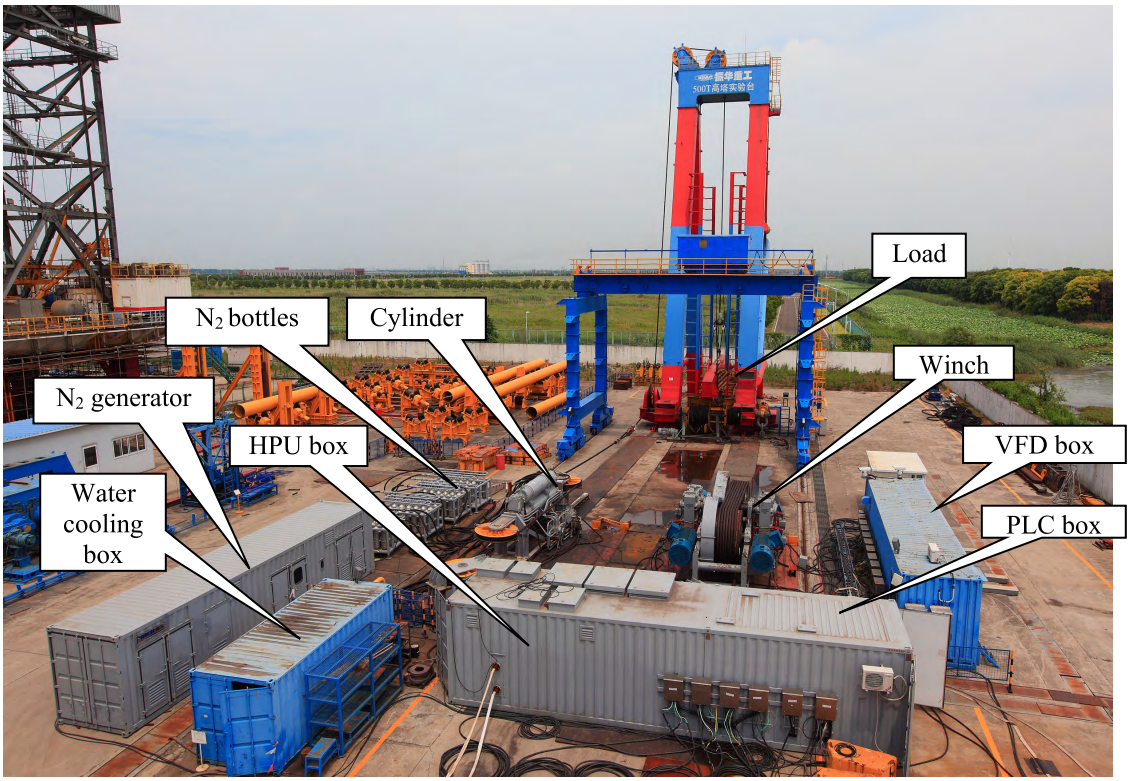

FIGURE 2. Full-scale 200 T semi-active heave compensation system.

A reasonable efficiency of the hydraulic system is 77% [3], [13]. Thus, the peak power of the semi-active system is roughly 5.01 MW.

Well-designed PHC devices can obtain efficiencies above 80 % [4], [6]. Thus, approximately 20 % space is left for the AHC parts. Consequently, a 1: 5 capacity ratio of PHCs to AHCs is a reasonable choice. The following assumptions are made: the active part shares 20 % of peak power, and the passive part shares 100 % peak power. As a result, the active part has a power of 1 MW and the passive part has a power of 5 MW.

III. SEMI-ACTIVE HEAVE COMPENSATION SYSTEM

A. SEMI-ACTIVE HEAVE COMPENSATION SYSTEM

The developed semi-active heave compensation system has a flying sheave structure [4], [14], as shown in Fig. 1. The winch is strictly a lowering and lifting equipment, and the integrated cylinder is strictly a heave compensation device.

The developed full-scale semi-active heave compensation system is shown in Fig. 2. The left side is the hydraulic system consisting of the integrated cylinder, the nitrogen bottles, the nitrogen generator, the water cooling equipment and the hydraulic power unit (HPU). The electrical system on the right consists of the winch, the load, the programmable logic controller (PLC), and variable frequency drives (VFDs). The winch and the integrated cylinder are shown in detail in Fig. 3.

FIGURE 3. Winch and integrated cylinder of the semi-active heave compensation system.

B. HYDRAULIC SYSTEM

The hydraulic system of the semi-active heave compensation system is shown in Fig. 4. The core of the hydraulic system is the integrated cylinder, which is controlled by the proportional valves.

The integrated cylinder has three chambers, among which A and B are active chambers, and C is the passive chamber (Fig. 4). Chambers A and B are connected with a proportional valve. Chamber C is linked with a gas accumulator. Chambers A and B have the same ram areas.

The integrated cylinder has an inner diameter of 0.54 m, its rod has a diameter of 0.48 m, and the chamber in the rod has a diameter of 0.25 m. The cylinder has a 3 m travel. With one wrap of the cable, a 6 m cable take-up and a $\pm$3m heave compensation ability are provided. The working pressure is 25 MPa. The integrated cylinder is manufactured by Bosch Rexroth Company from Netherlands.

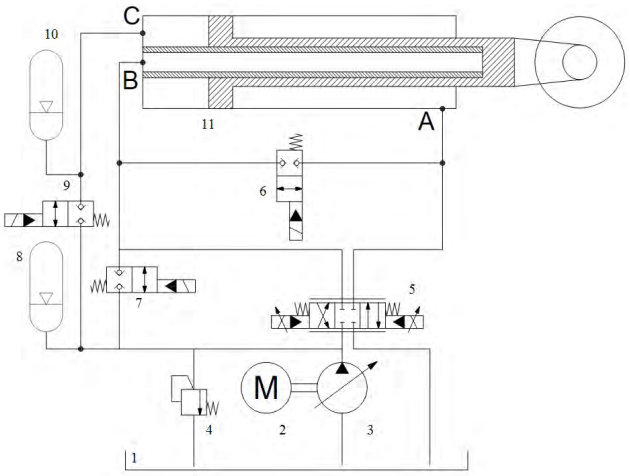

FIGURE 4. Hydraulic system of the semi-active heave compensation system. 1 Oil tank, 2 Three-phase motor, 3 Pump, 4 Safety valve, 5 Proportional valve 6 PHC connection valve, 7 PHC on-off valve, 8 Stabilizing accumulator 9 PHC accumulator prefill valve, 10 PHC accumulator, 11 Integrated cylinder.

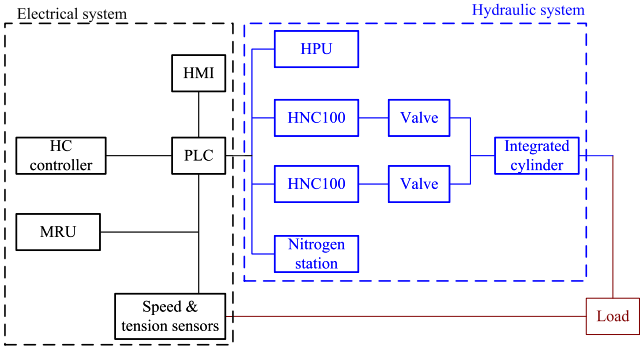

FIGURE 5. Electrical system of the semi-active heave compensation system.

The active chamber has a maximum working pressure of 28.5 MPa and a maximum flow of 2886 L/min. Thus, its maximum power is 1.37 MW. Three 355 kW motors are used to drive the pump.

The passive chamber has a working pressure ranging from 23 MPa to 28 MPa and a maximum flow of 10580 L/min. As a result, its maximum power is 4.94 MW. The PHC accumulator has a volume of 600 L.

C. ELECTRICAL SYSTEM

The electrical system of the semi-active heave compensation system is shown in Fig. 5. PLC is the control center that interfaces with the heave compensation (HC) controller, MRU, human-machine interface (HMI), speed and tension sensors, and the hydraulic system. HNC100 is the control center of the hydraulic system.

IV. CONTROL STRATEGIES

Control strategies of the semi-active heave compensation system are shown in Fig. 6 [15]–[17]. When the sea state is low, the heave compensation controller is cut off, and the feedback controller is used for lifting and lowering the load.

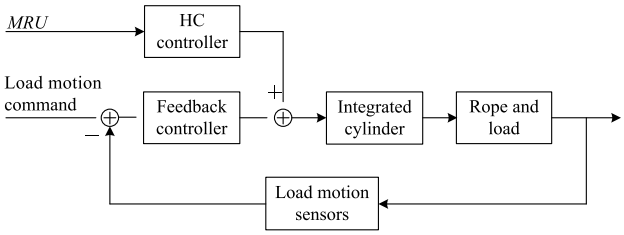

FIGURE 6. Control strategies of the semi-active heave compensation system.

When the sea state is high, the heave compensation controller is operated to compensate the heave motion.

The heave compensation controller is an extended PID controller with a speed outer loop and an acceleration inner loop. A speed related friction correction lookup table is embedded in the controller to reduce the influence of the cylinder friction. The table models a constant Coulomb friction, a square static friction, and a variable slope dynamic friction.

V. EXPERIMENTAL RESULTS

A. EXPERIMENTAL PROCEDURES

The full-scale factory testing layout of the semi-active heave compensation system is shown in Fig. 2.

A perfect sinusoidal wave with different periods and amplitudes from the MRU is set as the command input; the actual load attempts to track this sinusoidal wave. In other words, the command sinusoidal is the heave motion, and the tracking error is the residual heave motion. During the experiment, the cylinder displacements x_p and pressures are recorded for further analysis. The cable tension is monitored by sensors; however the tension data have not been recorded.

B. LOAD DISPLACEMENT ANALYSIS

Let x_L be the load displacement, and from Fig. 4, x_L is related to cylinder displacement x_p by

$$x_L = 2x_p. \tag{6}$$

The load is fixed at 200 T. The load position responses x_L of the semi-active system under wave periods of 8 s and 16 s at a wave amplitude of 2.5 m are shown in Figs. 7 and 8, respectively. The blue line is the command heave motion, the green line is the actual load position, the red line is the position error, and the purple lines are the 10 % error belt.

Both figures show that the actual load positions can track the command heave motion perfectly and the residual heaves are all within the 10 % error belts. Under a wave period of 16 s, Fig. 8 shows that the residual heaves exhibit a sinusoidal waveform superposed with 2 s fast oscillations. The reasons of the fast oscillations are given in Section V.C.

The maximum residual heaves at six typical working conditions are summarized in Table 2. The pie chart in Fig. 9 shows that the mean residual heave is 7.05 %, which meets the 10 % design requirement. Moreover, the semi-active system has a compensation efficiency of 92.9 %.

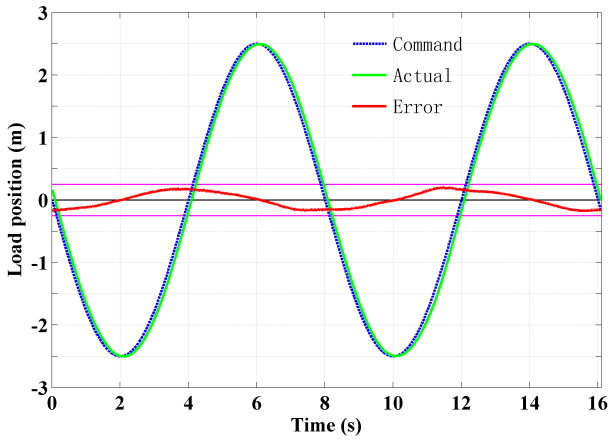

FIGURE 7. Position responses at a wave period of 8 s and a wave amplitude of 2.5 m of the semi-active heave compensation system.

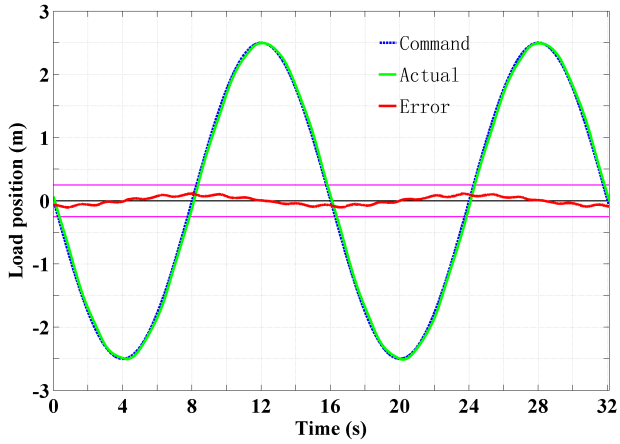

FIGURE 8. Position responses at a wave period of 16 s and a wave amplitude of 2.5 m of the semi-active heave compensation system.

TABLE 2. Residual heaves at typical working conditions of the semi-active heave compensation system.

Wave period (s)	Wave amplitude (m)	Maximum residual heave (m)	Maximum residual heave ratio (%)
8	1.5	0.112	7.46
8	2	0.182	9.11
8	2.5	0.208	8.34
10	2.5	0.169	6.78
16	1.25	0.0718	5.74
16	2.5	0.123	4.90
			7.05 (mean)

C. CYLINDER POWER ANALYSIS

The semi-active system consists of passive and active parts. The contribution of each part is an important issue and thus analyzed here in a power perspective.

The dynamics of the integrated cylinder is [9], [10]

$$m_{eq}\ddot{x}_p = p_A A_A - p_B A_B - p_C A_C - F_W - 2F_{cable}, \quad (7)$$

where m_{eq} is the equivalent mass of the load and the cable; x_p is the displacement of the integrated cylinder; p_A, p_B, and p_C are the pressures of chambers A, B, and C, respectively;

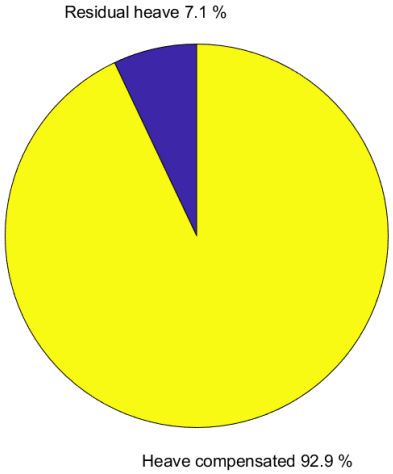

FIGURE 9. Efficiency of the semi-active heave compensation system.

A_A, A_B, and A_C are the ram areas of chambers A, B, and C, respectively; F_W is the damping and viscous friction forces on the cylinder rod.

Neglecting F_W, (7) is simplified to

$$m_{eq}\ddot{x}_p \approx p_A A_A - p_B A_B - p_C A_C - 2F_{cable}. \quad (8)$$

From (3), (8) is changed to

$$m_{eq}\ddot{x}_p \approx p_A A_A - p_B A_B - p_C A_C - 2W_L. \quad (9)$$

When the transient is settled and the dynamics of (9) is in a stable state, the left of (9) is close to zero, that is,

$$0 \approx p_A A_A - p_B A_B - p_C A_C - 2W_L. \quad (10)$$

Let v_p be the velocity of the cylinder. After multiplying v_p in both sides of (10), the force equation (10) is transformed into the power equation:

$$0 \approx p_A A_A v_p - p_B A_B v_p - p_C A_C v_p - 2W_L v_p. \quad (11)$$

Active chambers A and B have the same ram areas, that is $A_A = A_B$. From (6), the following condition is obtained:

$$v_L = 2v_p. \quad (12)$$

Equation (11) is changed to

$$\underbrace{W_L v_L}_{loadpower} \approx \underbrace{(p_A - p_B)A_A v_p}_{activepower} - \underbrace{p_C A_C v_p}_{passivepower}. \quad (13)$$

The pressure differences of the active chambers,$p_A - p_B$, and the cylinder velocity v_p are measured. Consequently, the power of the active chambers can be determined from (13). The load power can also be calculated from (13), and then the contribution of the active and passive chambers can be found.

Under a wave period of 8 s, the pressure differences of active chambers A and B show a largely sinusoidal waveform and the 2 s fast oscillations are negligible (Fig. 10a). As shown in Fig. 10b, the active chamber power shows a period of 4 s for the multiplication of the pressure and the speed from (13).

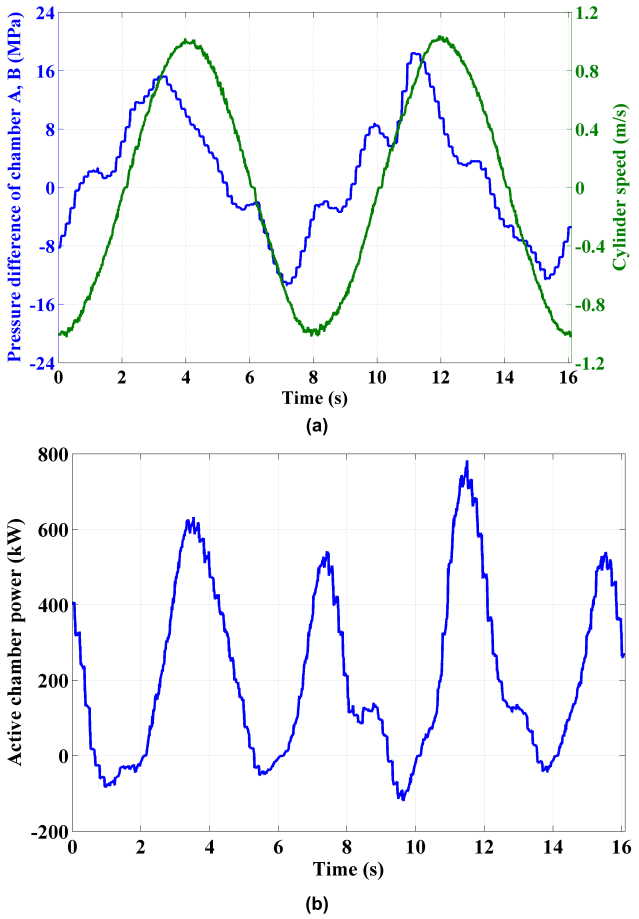

FIGURE 10. Pressure and power and cylinder speed of active chambers at a wave period of 8 s and a wave amplitude of 2.5 m of the semi-active heave compensation system. (a) Pressure difference of active chambers and cylinder speed. (b) Power of active chambers.

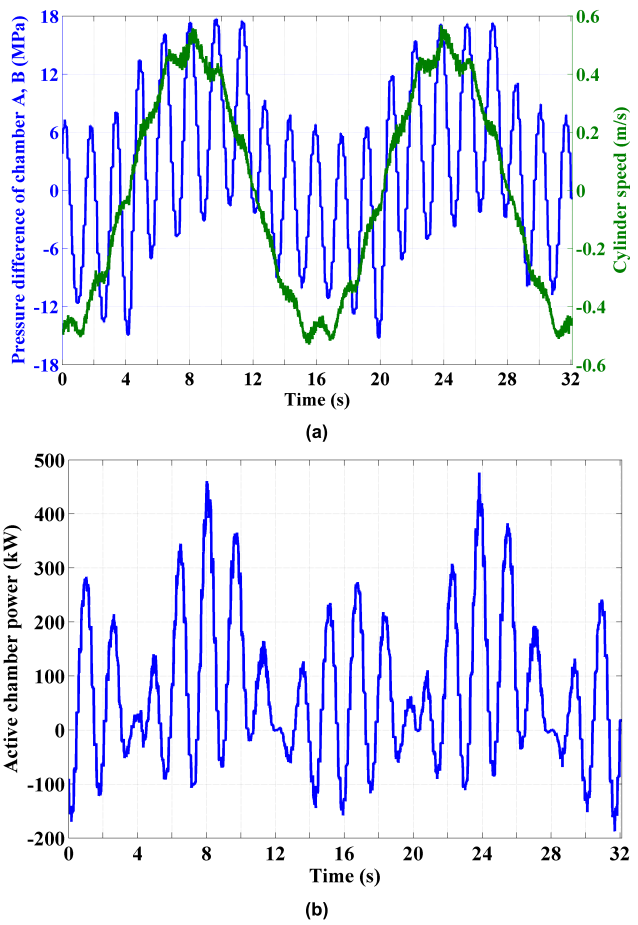

FIGURE 11. Active chambers' pressure and power and cylinder speed at a 16 s wave period and a 2.5 m wave amplitude of the semi-active heave compensation system. (a) Pressure difference of active chambers and cylinder speed. (b) Power of active chambers.

Under a wave period of 16 s, the pressure differences of active chambers A and B show a mainly sinusoidal waveform and the 2 s fast oscillations are considerable in Fig. 11a. The active chamber power also shows a period of 2 s as shown in Fig. 11b, which is chiefly determined by the fast oscillations. The pressure oscillations in Fig. 11a consist with the residual heave oscillations in Fig. 8.

Fourier analysis reveals [18] that the pressure spectrum has two main peaks, one centered at 0.0625 Hz (a 16 s period) with a 5.89 MPa amplitude, another centered at 0.625 Hz (a 1.6 s period) with a 7.63 MPa amplitude, Fig. 12a. The slow 0.0625 Hz oscillation comes from the external wave input and the cause for this fast 0.625 Hz oscillation will be analyzed later. The cylinder speed spectrum has only one peak centered at 0.0625 Hz with a 0.490 m/s amplitude, and the fast 0.625 Hz oscillation has a very weak amplitude of 0.0250 m/s. The power spectrum of active chambers has also two main peaks, one centered at 0.0625 Hz with a 55.0 kW amplitude, another centered at 0.563 Hz (a 1.78 s period) with a 115 kW amplitude, Fig. 12b.

The 2 s fast oscillations are related to the natural frequency of the integrated cylinder. The cylinder with accumulators in Fig. 4 may be viewed as an oil spring. The stiffness of an oil spring k is defined as [19]

$$k = \frac{nV_0^n A_C^2}{(V_0 - A_C x_p)^{n+1}} p_0, \tag{14}$$

where n is the polytropic index, V_0 is the PHC accumulator volume, and p_0 is the nitrogen pressure.

The natural frequency of an oil spring ω_n is [19], [20]

$$\omega_n = \sqrt{\frac{k}{m}}, \tag{15}$$

where m is the load mass.

In this study, $n = 1$, $V_0 = 600\ L$, $A_C = 0.167\ m^2$, $p_0 = 25\ MPa$, and $m = 200\ T$. From (14) and (15), this oil spring has a natural frequency of 0.385 Hz when x_p is 0 m and 0.662 Hz when x_p is 1.5 m which consists with the experimental fast oscillations frequencies of 0.563 Hz (Fig. 12b) and 0.625 Hz (Fig. 12a). The volume of the PHC accumulator may be decreased to increase the stiffness of this oil spring and improve the pressure responses. The PID heave compensation controller in Fig. 6 is designed with a relative large proportion factor to reduce the residual motion. However, this

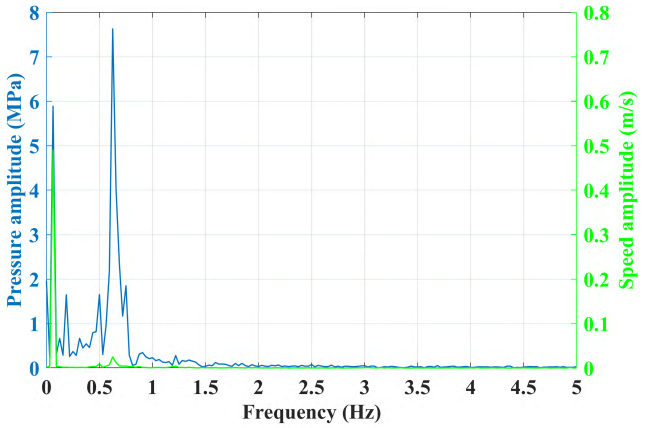

(a)

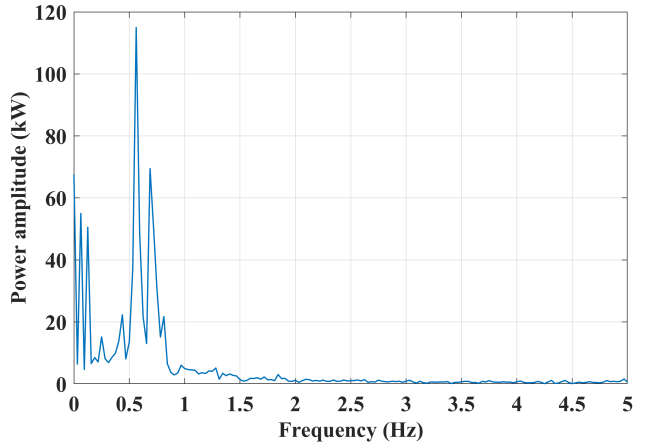

(b)

FIGURE 12. Fourier amplitude spectra of active chambers' pressure and power and cylinder speed at a 16 s wave period and a 2.5 m wave amplitude of the semi-active heave compensation system. (a) Amplitudes of pressure difference of active chambers and cylinder speed. (b) Power amplitude of active chambers.

TABLE 3. Active power at different conditions of the semi-active heave compensation system.

Wave period (s)	Wave amplitude (m)	Maximum load power (MW)	Maximum active power (MW)	Active power /Load power (%)
8	1.5	2.31	0.413	17.9
8	2	3.08	0.734	23.9
8	2.5	3.85	0.783	20.3
10	2.5	3.08	0.566	18.4
16	1.25	0.962	0.262	27.2
16	2.5	1.92	0.477	24.8
				22.1 (mean)

large proportion factor also amplifies noise, and the system is prone to triggering the natural frequency of the cylinder.

The maximum active powers at six different conditions are summarized in Table 3. At the wave period of 8 or 16 s, large wave amplitude indicates large active chamber power output. The mean ratio of the maximum active power to the maximum load power is 22.1 %. From (13), the contribution of the passive chamber is obtained as 77.9 %.

The pie chart in Fig. 9 shows that the semi-active system has a displacement compensation efficiency of 92.9 %.

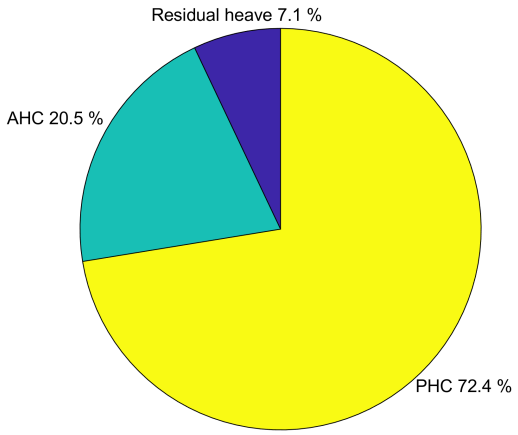

FIGURE 13. Contributions of AHC and PHC of the semi-active heave compensation system.

This result, combined with those of power analysis above, indicates that the contribution of the active chambers is 20.5 %, and the contribution of the passive chamber is 72.4 %. These observations are summarized in Fig. 13. The efficiency of the passive chamber consists with the 68 % – 80 % passive compensation efficiency from Oceanworks Company [4] and Rexroth Company [3], [6]. These observations allow a comprehensive understanding of the roles of the active and passive parts of a semi-active heave compensation system.

Figure 13 shows that, if the active system fails, then the semi-active heave compensation system will operate in the passive mode, and the system efficiency will degrade from 92.9 % to 72.4 %.

D. DAMPING COEFFICIENT OF THIS HEAVE COMPENSATOR

The damping coefficient of this semi-active heave compensator is [20]

$$\zeta = \frac{b+c}{2\omega_n m}, \tag{16}$$

where b is viscous damping coefficient, and c is the viscous friction coefficient of cylinder.

From (15), the natural frequency of the heave compensator ω_n is related to the stiffness k. From (14), k varies with the cylinder displacement. And thus, ζ is variable.

In addition, the heave compensation controller uses a speed related friction correction lookup table to reduce the influence of the cylinder friction. The lookup table models three types of friction, a constant Coulomb friction, a square static friction, and a variable slope dynamic friction.

Consequently, no effort is made to find the exact ζ, however ζ is set as 0.8 in a simulation research of this semi-active heave compensation system.

VI. CONCLUSION

The design philosophy of a semi-active heave compensation system for a 200 T winch is presented. An integrated cylinder with one passive chamber and two active chambers

is designed. The capacities of the passive and active chambers are determined. Full-scale factory tests at different wave periods and amplitudes show that the semi-active heave compensation system has a displacement compensation efficiency of 92.9 %, which meets the 90 % design requirement. In-depth power analysis shows that the active and passive chambers contribute the 20.5 % and 72.4 % heave compensation efficiency, respectively. The efficiency of the passive chamber consists with the 68 % – 80 % passive compensation efficiency from Oceanworks Company and Rexroth Company. If the active system fails, then the semi-active heave compensation system will operate in the passive mode, and the system efficiency will degrade from 92.9 % to 72.4 %. Further sea trials are needed to test the underwater performance of the semi-active heave compensation system.

ACKNOWLEDGMENT

The authors are grateful to the reviewers of this paper for their excellent comments.

REFERENCES

[1] L. Carral, J. de Lara Rey, J. C. Alvarez-Feal, and J. C. Couce, "Winch control gear for CTD sampling with a system to compensate vertical motion heave when manoeuvring in rough seas," *Ocean Eng.*, vol. 135, pp. 246–257, May 2017.

[2] W. Quan, Y. Liu, A. Zhang, X. Zhao, and X. Li, "The nonlinear finite element modeling and performance analysis of the passive heave compensation system for the deep-sea tethered ROVs," *Ocean Eng.*, vol. 127, pp. 246–257, Nov. 2016.

[3] J. K. Woodacre, R. J. Bauer, and R. A. Irani, "A review of vertical motion heave compensation systems," *Ocean Eng.*, vol. 104, pp. 140–154, Aug. 2015.

[4] A. Huster, H. Bergstrom, J. Gosior, and D. White, "Design and operational performance of a standalone passive heave compensation system for a work class ROV," in *Proc. OCEANS*, 2009, pp. 1–8.

[5] J. T. Hatleskog and M. W. Dunnigan, "Heave compensation simulation for non-contact operations in deep water," in *Proc. OCEANS*, 2006, pp. 1–6.

[6] Rexroth. (2017). *Heave Compensation Brochure*. Accessed: Sep. 2017. [Online], Available: https://dc-corp.resource.bosch.com/media/general_use/industries_2/machinery_applications_and_engineering/offshore/applications_8/heave_compensation/Heave-Compensation-Brochure.pdf

[7] J. T. Hatleskog and M. W. Dunnigan, "Active heave crown compensation sub-system," in *Proc. OCEANS-Europe*, 2007, pp. 1–6.

[8] S. Küchler, T. Mahl, J. Neupert, K. Schneider, and O. Sawodny, "Active control for an offshore crane using prediction of the vessel's motion," *IEEE/ASME Trans. Mechatronics*, vol. 16, no. 2, pp. 297–309, Apr. 2011.

[9] M. Richter, S. Schaut, D. Walser, K. Schneider, and O. Sawodny, "Experimental validation of an active heave compensation system: Estimation, prediction and control," *Control Eng. Pract.*, vol. 66, pp. 1–12, Sep. 2017.

[10] S. Z. Li, J. H. Wei, K. Guo, and W. L. Zhu, "Nonlinear robust prediction control of hybrid active-passive heave compensator with extended disturbance observer," *IEEE Trans. Ind. Electron.*, vol. 64, no. 8, pp. 6684–6694, Aug. 2017.

[11] W. Quan, Y. Liu, Z. Zhang, X. Li, and C. Liu, "Scale model test of a semi-active heave compensation system for deep-sea tethered ROVs," *Ocean Eng.*, vol. 126, pp. 353–363, Nov. 2016.

[12] L. R. Robichaux and J. T. Hatleskog, "Semi-active heave compensation system for marine vessels.," U.S. Patent 5 209 302, May 11, 1993.

[13] W. Pawlus, M. Choux, and M. R. Hansen, "Hydraulic vs. Electric: A review of actuation systems in offshore drilling equipment," *Model. Identificat. Control*, vol. 37, no. 1, pp. 1–17, 2016.

[14] J. E. Adamson, "Efficient heave motion compensation for cable-suspended systems," in *Proc. Underwater Intervent.*, New Orleans, LA, USA, 2003, pp. 1–7.

[15] T. A. Johansen, T. I. Fossen, S. I. Sagatun, and F. G. Nielsen, "Wave synchronizing crane control during water entry in offshore moonpool operations—Experimental results," *IEEE J. Ocean. Eng.*, vol. 28, no. 4, pp. 720–728, Oct. 2003.

[16] B. Skaare and O. Egeland, "Parallel force/position crane control in marine operations," *IEEE J. Ocean. Eng.*, vol. 31, no. 3, pp. 599–613, Jul. 2006.

[17] S. Messineo, F. Celani, and O. Egeland, "Crane feedback control in offshore moonpool operations," *Control Eng. Pract.*, vol. 16, no. 3, pp. 356–364, 2008.

[18] R. Wada, T. Kaneko, M. Ozaki, T. Inoue, and H. Senga, "Longitudinal natural vibration of ultra-long drill string during offshore drilling," *Ocean Eng.*, vol. 156, no, pp. 1–13, May 2018.

[19] S. Guo and Y. Yan, *Advanced Fluid Power Control*. Shanghai, China: Shanghai Scientific & Technical Publishers (in Chinese), 2017.

[20] W. H. C. Sanchez, T. M. Linhares, A. B. Neto, and E. L. F. Fortaleza, "Passive and semi-active heave compensator: Project design methodology and control strategies," *PLoS ONE*, vol. 12, no. 8, p. 26, Aug. 2017.

WANGQIANG NIU received the B.E. degree from Xi'an Aerotechnical College, Xi'an, China, in 1998, the M.E. degree from Northwestern Polytechnical University, Xi'an, in 2004, and the Ph.D. degree from Shanghai Jiao Tong University, Shanghai, China, in 2008.

He has been a Lecturer, since 2008, and an Associate Professor, since 2017, with Shanghai Maritime University, Shanghai, China. From 2013 to 2014, he is a Visiting Lecturer with McMaster University, Hamilton, ON, Canada. His research interests include control of marine equipment (ships and cranes), and wireless power transfer.

WEI GU received the B.E. and Ph.D. degrees from Shanghai Maritime University, Shanghai, China, in 1982 and 2008, respectively. He has been a Teacher with Shanghai Maritime University, since 1982, and a Professor, since 1997, where he is currently the Director of the Key Laboratory of Transport Industry of Marine Technology and Control Engineering. His research interest includes marine information control technology.

YUNFU YAN is currently the Chief Engineer of Shanghai Zhenhua Heavy Industry Co., Ltd, Shanghai, China. His research interest includes developments of offshore and harbor equipment.

XIANGYANG CHENG received the B.E. degree from the Wuhan University of Technology, Wuhan, China, in 1999.

He is currently a Senior Electrical Designer of Shanghai Zhenhua Heavy Industry Co., Ltd, Shanghai, China. His research interest includes developments of offshore heavy equipment.